NSE TECHINCAL TRANSACTION VOL. 44, N0.4, OCT – DEC., 2009
EMEKA S. OBE, DAMIAN B. NNADI AND J. EKE

INDUCTANCES AND AIRGAP FLUX DENSITY OF A SYNCHRONOUS RELUCTANCE MACHINE USING THE ACTUAL MACHINE GEOMETRY

BY

EMEKA S. OBE*, DAMIAN B. NNADI* AND J. EKE**

*Department of Electrical Engineering, University of Nigeria, Nsukka.
**Department of Electrical & Electronic Engineering, Enugu State University of Science and Technology, Enugu,

ABSTRACT

This paper reports the direct utilization of the actual rotor and stator geometry and winding placement patterns of a cageless synchronous reluctance machine to calculate its radial airgap flux density distribution and inductances. Analytical expressions representing machine winding functions and non-uniform airgap are derived in detail. The new method of computing the inductances and airgap flux density using this actual geometry and windings are based on the old concept of winding functions (WF). The procedure developed here does not rely on Fourier series expressions for airgap or winding, therefore complicated integrations are avoided. The effects of stator slots are included by considering them as added airgaps in its actual shapes and position not approximated forms that use Carter's coefficients. The rotor pole faces are modeled in the tapered manner in which they are made, considering the airgap along the pole arc as not being uniform. The inductances obtained are transformed to d-q-0 reference frame and the results are seen to compare favorably with finite-element (FE) calculations and measurements. Cross-coupling effects between the d-axis and q-axis inductances which finite element or the traditional measuring techniques are unable to identify are readily yielded by the proposed direct WF method.

Index Terms— winding function, radial flux density, inductances, slots, airgap function, synchronous reluctance machine

1.0 INTRODUCTION

The winding function theory was first reported in 1950 [1]. However, this powerful tool seemed to have been ignored in the following 30 years as it was from the 90's that an interest on using it was rekindled. Ever since then winding function theory has been used with success to calculate the inductances of induction and synchronous machines with constant or variable air gap length with or without rotor eccentricities [3]. The procedure is only second to finite-element methods [2] and recent reports [3] – [6] actually show that it has the potential of becoming as accurate and it also has other additional features. The beauty of the procedure is that given only the winding distribution and machine geometry, all machine inductances, airgap flux density and hence torque for any kind of excitation (balanced or unbalanced) can be computed. Since it yields all machine inductances in direct phase variables, it then lends itself readily to applications in fault diagnosis and analysis, eccentricity behavior, and other imaginable irregularities that may occur during the operation of an ac machine.

1.1 Derivation of winding functions

The expression for obtaining the winding function expression from winding distribution is readily available in literature but its derivation is very rare to find. The derivation is presented in this section using the concept of magnetic fields. A general equation for winding function that can be applied under any air gap condition will be found at the end of this section. Now consider for generality, an electric machine shown in Fig. 1, in which the air gap is not uniform. A closed area including stator core, air gap and rotor core is arbitrarily chosen and its boundary is shown as a dashed line in the figure, where AB is in the stator core; O is the central point of stator; OA and OB go through the rotor, air gap and stator core and can be considered to be orthogonal to the inner surface of the stator. Based on the Ampere's Law, the magnetic field (H) on the boundary AOB can be expressed in terms of the current density J, differential axial length dl and area ds as:

$$\oint_C H \cdot dl = \int_S J \cdot ds \qquad (1)$$

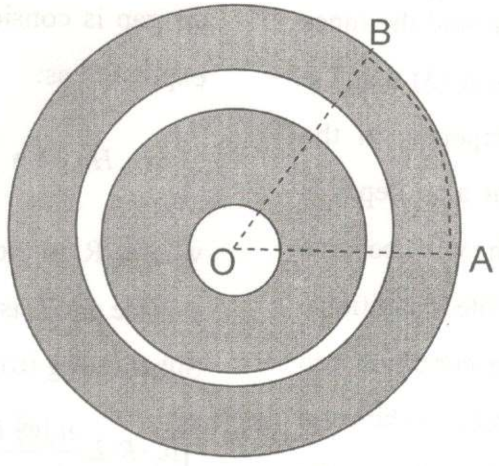

Fig. 1: An arbitrary electric machine showing non-constant air gap length

The length dl is an elemental length of the machine looking into the paper. If the turn function (defined as absolute mmf per unit ampere) of an arbitrary winding A can be modeled as an equation $n_A(\varphi)$, where φ is the angle around the inner surface of the stator, then (1) can be re-written as:

$$\oint_C H \cdot dl = n_A(\varphi) \cdot i_A \quad (2)$$

There are three important assumptions that need to be made before we can proceed:

(a) The air gap is so small compared to the stator or rotor core, such that the magnetic field in the air gap can be considered to be orthogonal to the inner surface of the stator. This is a very fundamental assumption in electric machine analysis and it permits the usage of a developed model of the machine.

(b) The permeability of iron is much larger than that of the air gap, such that the magneto-motive force drops on the stator core and the rotor core can be ignored. This allows for computation of entire torque at the airgap by integrating the Maxwell's stress tensor (measurable by the airgap flux density).

(c) Rotor and stator slot openings and fringing are ignored and assumed to be accounted for by Carter's coefficients. This assumption applies to the sinusoidal model which uses the derived winding and airgap functions and not to the actual model which uses the machine geometry and actual winding placement positions.

With these in mind, the general definition for the air gap is expressed as [4]:

$$g(\varphi,\theta_r) = g_0[1 - a_1\cos(\varphi+\gamma) - a_2\cos(\varphi-\theta_r+\gamma)] \quad (3)$$

where, a_1 and a_2 are constants, which represent the degree of static and dynamic eccentricity respectively; θ_r is the rotor mechanic angle; g_0 is the average air gap and angle γ can be used to change the distribution of the air gap around the inner stator surface. It is clear from (3) that the air gap length not only depends on the angle around the stator, but also depends on the rotor angle, which will be true under almost all the possible conditions. The uniform air gap length condition can be achieved by setting a_1 and a_2 to be zero. Applying the first two assumptions, the left-hand side of (2) can be restated as:

$$\oint_C H \cdot dl = H_A(\varphi) \cdot g(\varphi, \theta_r) - H_A(0) \cdot g(0, \theta_r) \qquad (4)$$

where, $g(0,\theta_r)$ is the air gap at the starting point and the value of φ at the starting point is assumed to be zero. $H_A(0)$ is the magnetic field at the starting point while $g(\varphi, \theta_r)$ and $H_A(\varphi)$ are the air gap length and magnetic field at φ angle point respectively.

Substituting (4) into (2),

$$H_A(\varphi) \cdot g(\varphi, \theta_r) - H_A(0) \cdot g(0, \theta_r) = n_A(\varphi) \cdot i_A \qquad (5)$$

An expression for the magnetic field around the stator can be factored from (5) as:

$$H_A(\varphi) = \frac{n_A(\varphi) \cdot i_A + H_A(0) \cdot g(0, \theta_r)}{g(\varphi, \theta_r)} \qquad (6)$$

The value of magnetic field is the objective, however, one equation cannot solve two unknown variables $H_A(\varphi)$ and $H_A(0)$ from only (6). So Gauss's Law is applied here to get another constraint equation. If a cylinder passing through the air gap is considered, Gauss's Law can be expressed as:

$$\int_0^{2\pi} \mu_0 H_A(\varphi) \cdot R \cdot L \cdot d\varphi = 0 \qquad (7)$$

where, R is the radius of the inner stator surface and L is the length of the machine.

Substituting (6) into (7),

$$\int_0^{2\pi} \mu_0 \cdot R \cdot L \cdot \frac{n_A(\varphi) \cdot i_A + H_A(0) \cdot g(0, \theta_r)}{g(\varphi, \theta_r)} d\varphi = 0 \qquad (8)$$

Since none of R, L or μ_0 is zero, (8) can be rearranged to:

$$H_A(0) \cdot g(0, \theta_r) = -\frac{\int_0^{2\pi} \frac{n_A(\varphi)}{g(\varphi, \theta_r)} d\varphi}{\int_0^{2\pi} \frac{1}{g(\varphi, \theta_r)} d\varphi} \cdot i_A \qquad (9)$$

Substituting (9) into (6),

$$H_A(\varphi) = \frac{n_A(\varphi) \cdot i_A}{g(\varphi, \theta_r)} - \frac{1}{g(\varphi, \theta_r)} \frac{\int_0^{2\pi} \frac{n_A(\varphi)}{g(\varphi, \theta_r)} d\varphi}{\int_0^{2\pi} \frac{1}{g(\varphi, \theta_r)} d\varphi} \cdot i_A \qquad (10)$$

If the definition of the winding can be expressed as:

$$N_A(\varphi) \cdot i_A = H_A(\varphi) \cdot g(\varphi, \theta_r) \qquad (11)$$

Then the general winding function can be found as:

$$N_A(\varphi) = n_A(\varphi) - \frac{\int_0^{2\pi} \frac{n_A(\varphi)}{g(\varphi, \theta_r)} d\varphi}{\int_0^{2\pi} \frac{1}{g(\varphi, \theta_r)} d\varphi} \qquad (12)$$

If the air gap is uniform, which means that , the winding function in equation (12) can be simplified as:

$$N_A(\varphi)=n_A(\varphi)-\frac{\int_0^{2\pi}\frac{n_A(\varphi)}{g_0}d\varphi}{\int_0^{2\pi}\frac{1}{g_0}d\varphi}=n_A(\varphi)-\frac{\int_0^{2\pi}n_A(\varphi)d\varphi}{2\pi}=n_A(\varphi)-\langle n_A(\varphi)\rangle \quad (13)$$

where $\langle n_A(\varphi)\rangle$ is the average of the turn function. This result matches with the one that can be found in the papers considering uniform air gap.

If the airgap is not uniform, the integration in the winding function calculation becomes involving but the inverse of the air gap can be approximated as:

$$\frac{1}{g(\varphi,\theta_r)}=A_0+\sum_{i=1}^{\infty}A_i\cos(i\varphi-i\theta_r'+i\gamma) \quad (14)$$

where, $A_0=\dfrac{1}{g_0\sqrt{1-a_3^2}}$,

$$A_i=\frac{2}{g_0\sqrt{1-a_3^2}}\cdot\left(\frac{1-\sqrt{1-a_3^2}}{a_3}\right)^i,$$

$a_3=\sqrt{a_1^2+2a_1a_2\cos\theta_r+a_2^2}$ and

$$\theta_r'=\arctan\left(\frac{a_2\sin\theta_r}{a_1+a_2\cos\theta_r}\right).$$

Generally, for a three phase machine excited with a pure sinusoidal supply, only the first two terms are used as an approximation as:

$$\frac{1}{g(\theta,\theta_r)}=A_0+A_1\cos(\theta-\theta_r'+\gamma) \quad (15)$$

If the expression for the inverse of the air gap is now substituted into the general winding function equation, a new simplified expression of winding function will be achieved as:

$$N_A(\varphi)=n_A(\varphi)-\langle n_A(\varphi)\rangle-\sum_{i=1}^{\infty}\frac{A_i}{2\pi A_0}\int_0^{2\pi}n_A(\varphi)\cos(i\varphi-i\theta_r'+i\gamma)d\varphi \quad (16)$$

Equation (16) even though representing a simplified model leads to some algebraic difficulties even for the simplest cases. One of the authors of the present paper has proposed a faster and more accurate method [6] in which all terms of (14) and (16) are used without any need for algebraic expressions. The same method is used here in the actual model calculations but the emphasis in this paper is that the above derivation was lacking in the past work and there also exists a need to show the airgap flux densities calculated by the new and conventional procedures using the actual rotor pole arc shapes.

The above derivation was performed for a machine with cylindrical rotor and hence is valid for round rotor synchronous and induction machines even under eccentricity conditions. For a reluctance machine, the rotor must have salient poles and hence the inverse airgap function is modeled as:

$$g^{-1}(\phi,\theta_r)=\frac{1}{2}\left(\frac{1}{g_1}+\frac{1}{g_2}\right)-\frac{2}{\pi}\left(\frac{1}{g_1}-\frac{1}{g_2}\right)\sin(\pi\beta)\cos 2(\phi-\theta_r) \quad (17)$$

In (17) g_1 and g_2 are the airgap at pole face and depth between poles respectively and β is the ratio of pole arc to pole pitch.

1.2 Derivation of inductance expression

A general expression for the inductance calculation is necessary and even though this expression is widely known, its derivation is also not available in literature. From the winding function theory, the inductances can be calculated using winding and turn functions of the windings. If the winding function of A^{th} winding is expressed as $N_A(\varphi)$, where φ is the angle around the stator, then the magnetic field around the stator can be expressed as:

$$H_A(\varphi)=\frac{N_A(\varphi)}{g(\varphi,\theta_r)}\cdot i_A \tag{18}$$

where, $g(\varphi, \theta_r)$ is the air gap function and i_A is the current flowing through winding A. Then the flux density in the air gap due to the current in winding A can be written as:

$$B_A(\varphi)=\mu_0\frac{N_A(\varphi)}{g(\varphi,\theta_r)}\cdot i_A \tag{19}$$

Assume the mutual inductance between winding A and B is required and the winding function of B winding is $N_B(\varphi)$. The flux linkage induced in winding B due to the winding A current i_A can be expressed as:

$$\lambda_{BA}=\mu_0\cdot R\cdot L\cdot i_A\cdot\int_0^{2\pi}\frac{1}{g(\varphi,\theta_r)}\cdot N_B(\varphi)\cdot N_A(\varphi)\cdot d\varphi \tag{20}$$

where, R is the mean value of radius of the air gap middle line and L is the effective length of the stator core.

Since the definition of the mutual inductance is:

$$L_{BA}=\frac{\lambda_{BA}}{i_A} \tag{21}$$

The general expression for the mutual inductance calculation is:

$$L_{BA}=\mu_0\cdot R\cdot L\int_0^{2\pi}\frac{1}{g(\varphi,\theta_r)}\cdot N_B(\varphi)\cdot N_A(\varphi)\cdot d\varphi \tag{22}$$

The inductances considered here in (22) also include the stator winding self-inductances and the mutual inductances between the stator windings.

2.0 Inductance and Flux Density Calculations

2.1 Winding layout modeling

The machine under consideration has 36 stator slots a 4 pole rotor. The winding arrangement for one pole pitch is shown in Fig. 2. It is easy to decipher the winding arrangement for the entire machine by repeating the developed diagram for the remaining 3 poles. The machine geometric data is shown in Table I.

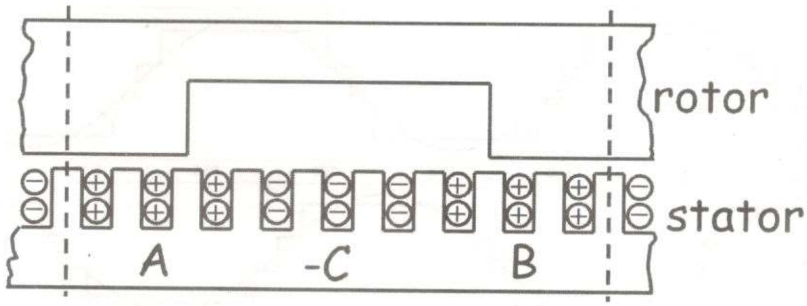

Fig. 2: Winding pattern

The turn function for the three phase winding can be drawn from Fig. 2 and is shown in Fig. 3. By following the procedure in section (1.1), the winding function can be obtained by removing the average of the turn function from itself as given in (13). This will yield Fig. 4

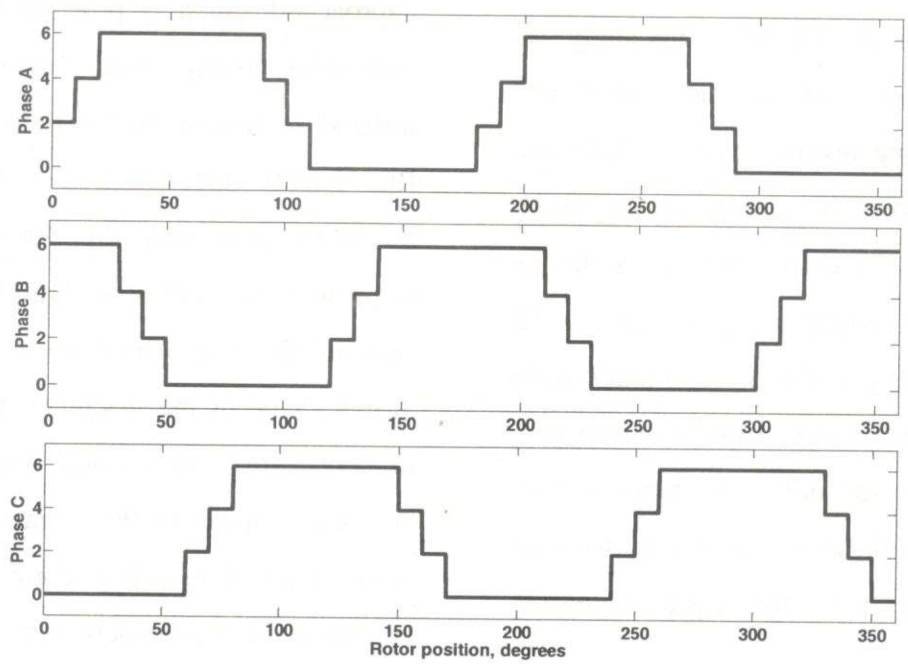

Fig.3: Turn functions for the three phases

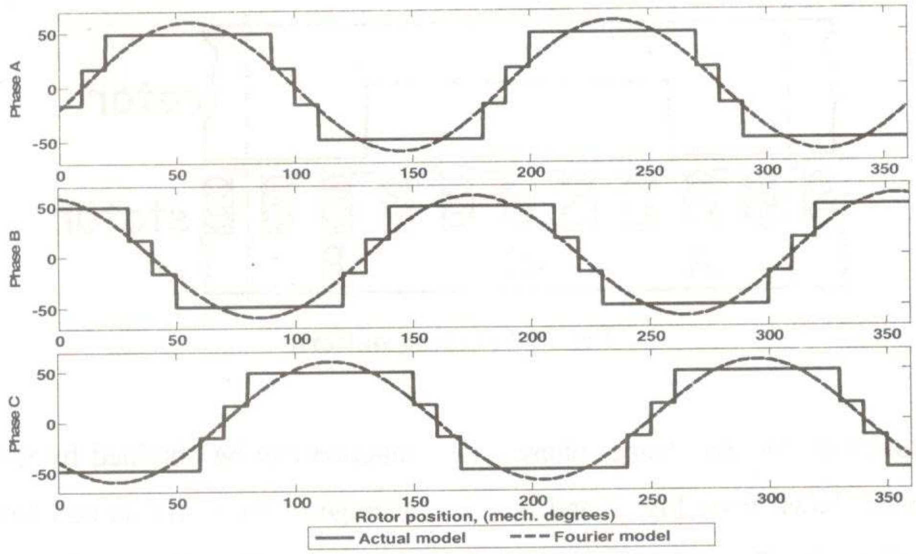

Fig. 4: Winding functions, actual and Fourier series model

2.2 Rotor airgap and pole modeling

The machine considered in this study has no rotor cage and can be started and operated using inverter control. Although the rotor poles has been shown to be rectangular (assuming the poles to be circular and airgap at pole face to be uniform) in Fig. 2, this representation is far from the actual rotor shape in salient-pole machines. Rotor poles are tapered such that the middle of the pole has the least airgap value with the airgap increasing gradually as the interpolar region is approached. Such a pole gives a more sinusoidal airgap flux density and is utilized in this study for inductance and flux density calculations. Fig. 5(a) shows the stator slots while Fig. 5(b) shows the rotor with tapered pole. Fig. 5(c) is the sum of the two which gives the actual airgap shape of the machine. Also shown in Fig. 5(c) on dashed lines is the sinusoidal model of the airgap using (17) with values of g_1 and g_2 corrected by the appropriate Carter's coefficients.

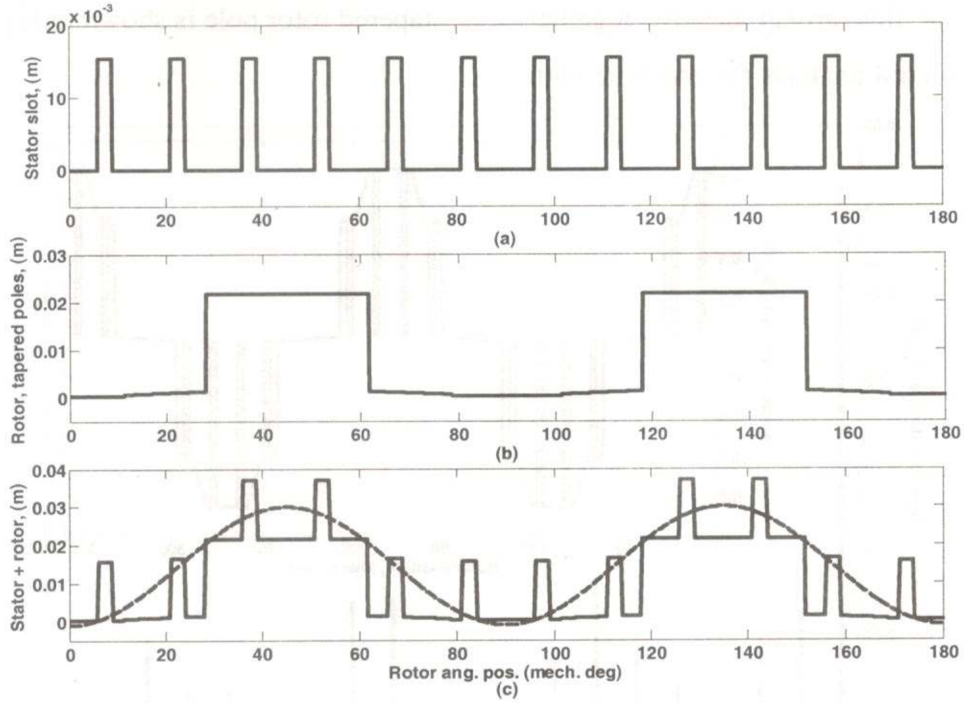

Fig. 5: Actual rotor pole shape, (a) stator slot openings, (b) rotor (with tapered poles), and (c) summation of stator slot openings and rotor airgap

TABLE I: Machine Dimensions

Quantity	Value
Stator Outer/Inner diameter	150/92.7mm
Machine stack length	90mm
Number of slots	24
Number of conductors per layer	17
Main airgap length g_1	0.3mm
Inter-polar slot space g_2	14.0mm
Stator slot depth	18.4mm
Ratio pole arc/pole pitch	2/3
Number of poles	4

2.3. Flux density distribution

Now consider a three-phase sinusoidal current given by:

$$\begin{aligned} I_A &= I_p \cos(\theta_r + \kappa) \\ I_B &= I_p \cos(\theta_r - 2\pi/3 + \kappa) \\ I_C &= I_p \cos(\theta_r - 4\pi/3 + \kappa) \end{aligned} \qquad (23)$$

where $I_p = \sqrt{2} I_{rms}$ and κ is the current phase angle. The three-phase instantaneous value of current at any instant is such that $I_A + I_B + I_C = 0$, for example if I_A= 4.0A, then $I_B = I_C = -2$A is satisfactory.

The instantaneous radial airgap flux density distribution due to three phase excitation current for a particular value of rotor position, θ_r can be obtained from:

$$B_r(\varphi,\theta_r) = \mu_0 \frac{N_A(\varphi)I_A + N_B(\varphi)I_B + N_C(\varphi)I_C}{g(\varphi,\theta_r)} \qquad (24)$$

The plot of this airgap density together with its spectral analysis for machine with tapered rotor pole is shown in Fig. 6(a).

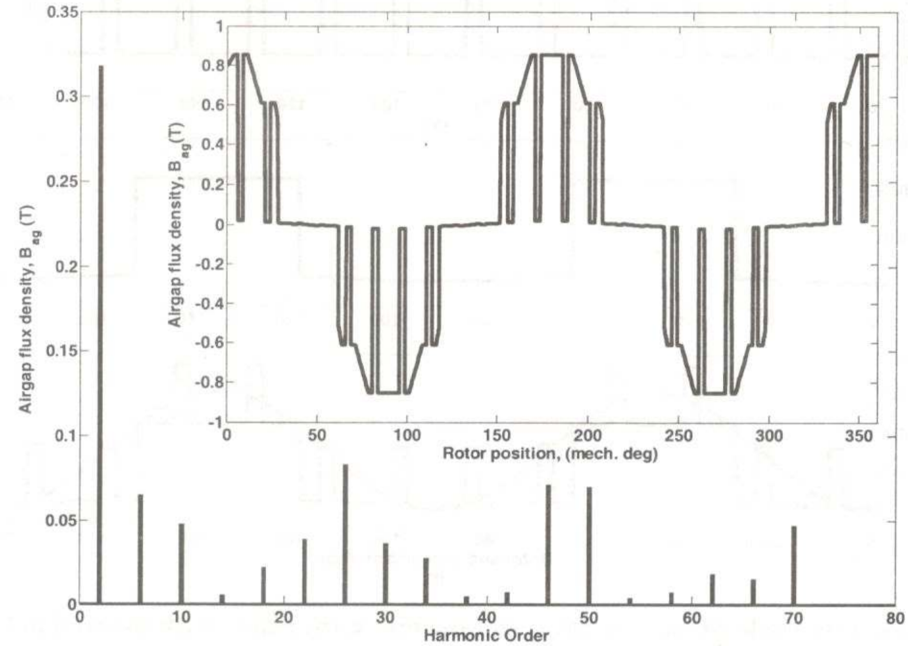

(a) Actual model

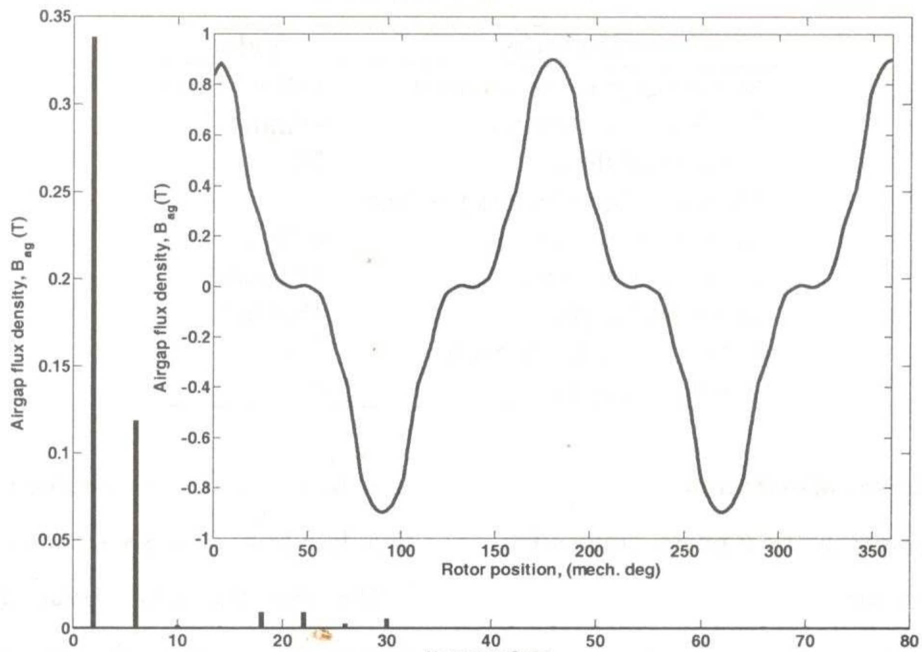

(b) Sinusoidal model

Fig. 6: Radial airgap flux density

In Fig. 6(b) is also shown the flux density distribution obtained from the sinusoidal model and their corresponding harmonic analysis. The actual model is richer in harmonics but the sinusoidal model has a slightly higher fundamental value.

2.4 Inductance calculation

The flow chart shown in Fig. 7 is sufficient for following the method of calculating the inductances and airgap flux density as discussed here. The procedure begins by definition of stator slots, the airgap (rotor) and the windings in such a manner that each vector (or data) representing all of them have the same length with the entire stator and rotor periphery. The integration in (22) is then performed by addition using (23) in which G is the effective airgap value resulting from addition of rotor geometry for a particular rotor position and stator slots.

$$L_{XY}(j) = \mu_o r l \left(\sum_{i=1}^{n \times m} \frac{N_X(i) N_Y(i)}{G(i,j)} \right) \qquad (25)$$

The effective airgap changes shape but maintains a constant area for each rotor position. The inductances computed by this procedure are shown in Fig. 8(a) where the effects of the slots are seen to be more pronounced in the self inductances. The presence of slots produces a waveform with frequency equal to the slot-pitch which modulates the inductance waveform. Fig.8(b) shows the corresponding results obtained from the sinusoidal model.

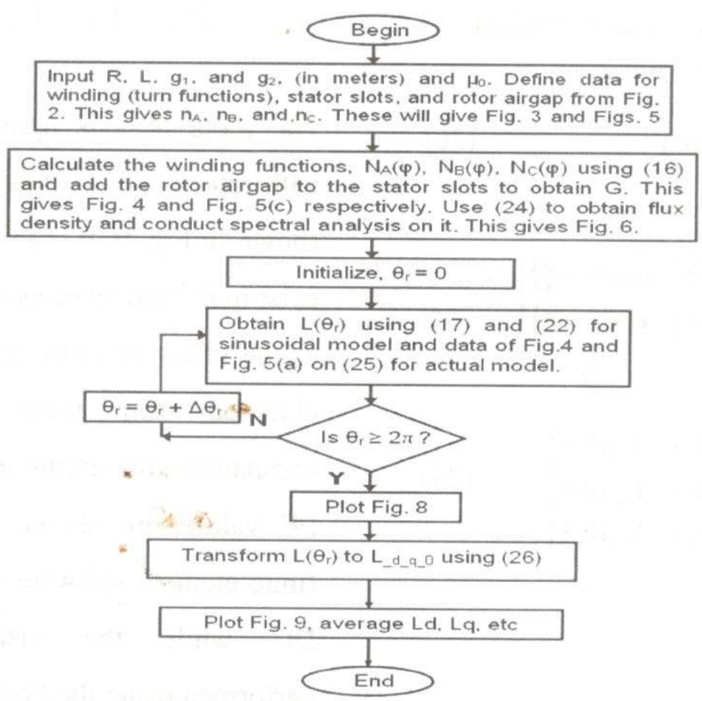

Fig. 7: Flow chart illustrating a summary of the calculation procedure

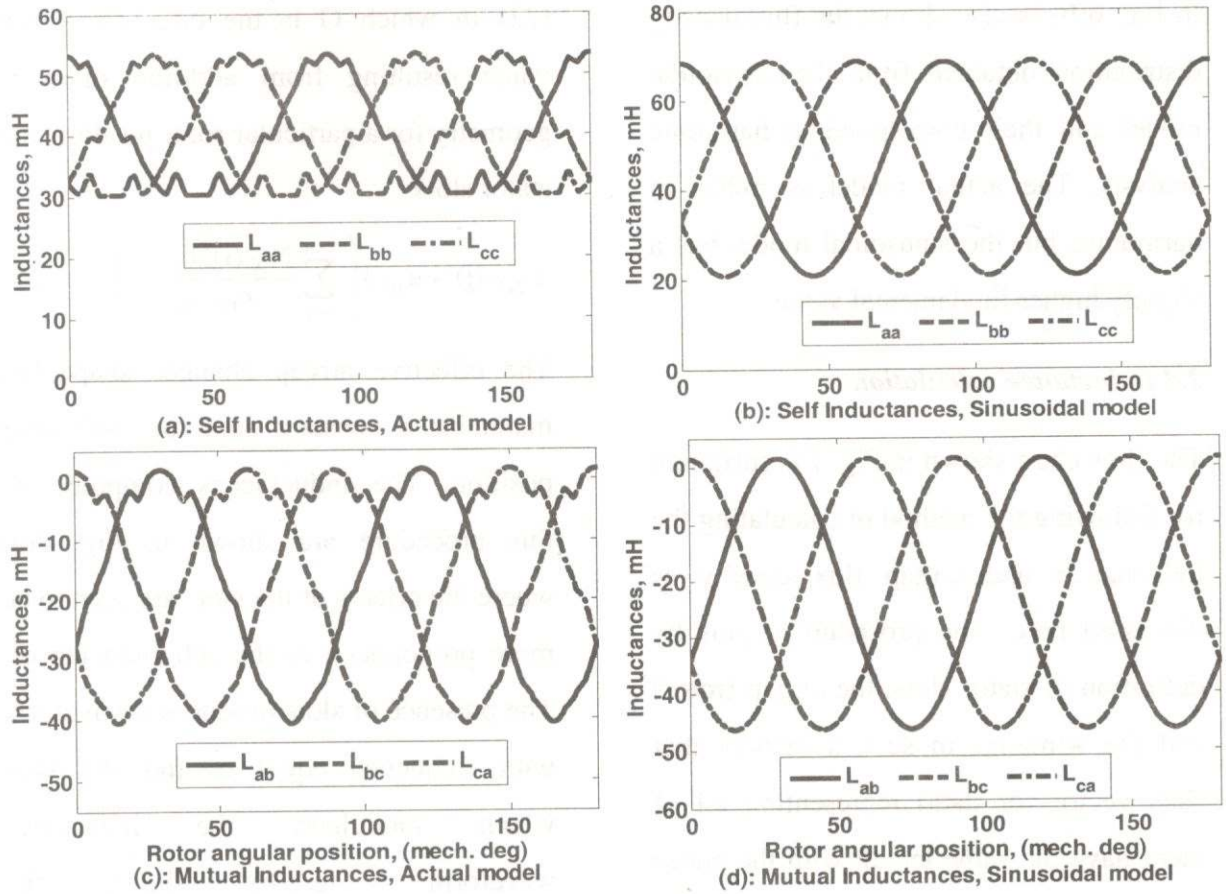

Fig. 8: Phase Inductances

3.0 Transformations to d-q-0 Frame

In order to obtain the d-q-0 values of the inductances, Park's transformation is performed with:

$$L_{d-q-0} = T(\theta_r)L(\theta_r)T(\theta_r)^{-1} \tag{26}$$

where:

$$T(\theta_r) = \begin{bmatrix} \cos\theta_r & \cos\left(\theta_r - \frac{2\pi}{3}\right) & \cos\left(\theta_r - \frac{4\pi}{3}\right) \\ \sin\theta_r & \sin\left(\theta_r - \frac{2\pi}{3}\right) & \sin\left(\theta_r - \frac{4\pi}{3}\right) \\ \frac{1}{\sqrt{2}} & \frac{1}{\sqrt{2}} & \frac{1}{\sqrt{2}} \end{bmatrix} \tag{27}$$

$$L(\theta_r) = \begin{bmatrix} L_{aa}(\theta_r) & L_{ab}(\theta_r) & L_{ac}(\theta_r) \\ L_{ba}(\theta_r) & L_{bb}(\theta_r) & L_{bc}(\theta_r) \\ L_{ca}(\theta_r) & L_{cb}(\theta_r) & L_{cc}(\theta_r) \end{bmatrix} \tag{28}$$

$$L_{d-q-0} = \begin{bmatrix} L_{dd} & L_{dq} & L_{d0} \\ L_{qd} & L_{qq} & L_{q0} \\ L_{0d} & L_{0q} & L_{00} \end{bmatrix} \tag{29}$$

The plots of axis inductances' variation with rotor position obtained using (26) are shown in Fig. 9. It is seen that ripples also exist in the inductances and this is still due to the effect of slots. The average values obtained from these calculations are compared with unsaturated measured and FE values are shown in Table II. The finite-element software used was FEMAG DC while the measurements were performed using the Fock and Hart method

[7]. If it is desired to obtain the d- and q-axis flux linkages, it then necessitates that (24) be evaluated separately for each of the phases A, B and C while setting the other two to zero, in turns. The resulting 3-phase flux densities can then be transformed to d-q-0 using (27).

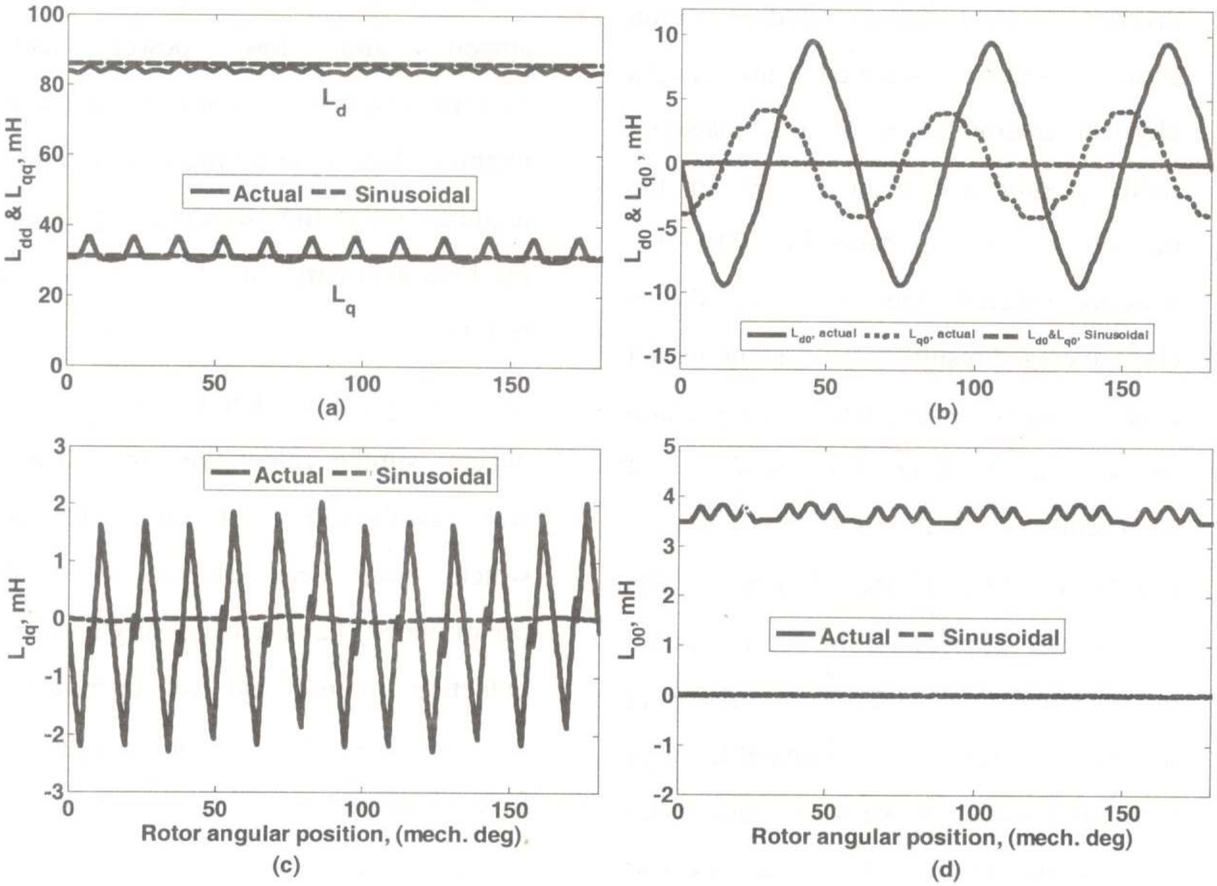

Fig. **9: Axis inductances, (a) L_d & L_q, (b) L_{q0} & L_{d0}, (c) L_{dq} and (d) L_{00}**

TABLE II

Resulting averaged values of the axis Inductances

Para-Meter	Calculated(mH)			Measured(mH)
	Sinusoidal	Actual	FE	
L_d	86.02	84.33	83.8	83.3
L_q	31.99	31.31	30.2	30.5
L_{dq}	0.0	0.175	-	-
L_{00}	0.0	3.63	-	-

4.0 Conclusion

This paper has presented the results of calculations and measurements of inductances and radial flux density of a synchronous reluctance motor designed for inverter operation. The detailed derivation shown in section 1 is aimed at providing a physical interpretation of the magnetic fields phenomena as it relates to the method of winding functions. The two winding function methods have shown close averaged results but the actual model reveals results varying with rotor position on account of stator slot openings and rotor saliency. In all cases, the measured results are closer to the FE results. The inclusion of tapering on the rotor pole arc in the actual model helped in arriving at results that are very comparable with sinusoidal model unlike a previous paper [6] in which the pole arc was assumed to be uniformly circular over the pole face.

Even though the airgap flux densities calculated by the two WF procedures display waveforms of differing shape, its harmonic analysis shows that both have very close values of fundamental components. It is only this component which is responsible for torque production if the supply is also perfectly sinusoidal. The kind of motor studied here has a low L_d/L_q ratio which implies that the machine performance will exhibit poor torque per ampere and low power factor, nevertheless, this paper has shown that WF method which is less time consuming and requires only the winding layout and machine geometry can also yield accurate results.

It is intended to demonstrate in future papers similar calculations for machines with axially-laminated rotor structures which have been shown to exhibit performance characteristics very similar to induction motors and yet operating at synchronous speed without magnets or field windings.

5.0 References

1. N. L. Schimtz and D. W. Novotny, *Introductory Electromechanics*, New York: The Ronald Press Company, 1950.

2. N Bianchi, *Electrical machines analysis using finite elements*, Boca Raton: Taylor and Francis CRC, 2005.

3. H. A. Toliyat and Nabil A. Al-Nuaim "Simulation and Detection of Dynamic Air-Gap Eccentricity in Salient-Pole Synchronous Machines", *IEEE Trans. Ind. Appl.*, Vol. 35, No. 1, pp.86–93, Jan/Feb, 1999.

4. Z. Wu and O. Ojo, "Modeling of a Dual Stator Winding Induction Machine Including the Effect of Main Flux Linkage Magnetic Saturation," *Conference Record of the Industry Applications Society Annual meeting*, Oct. 8-12, 2006, Tampa, Florida, USA.

5. T. Lubin, T. Hamiti and A. Rezzoug, "Comparison between Finite-element and Winding Function Theory of Inductances and Torque Calculation of a Synchronous Reluctance Machine" *IEEE Trans. Magnetics*, Vol. 43. No 8, p. 3406–3410, Aug. 2007.

6. E. S. Obe, "Direct computation of ac machine inductances based on winding function theory", *Energy Conversion and Management,* Vol. 50, Issue 3, pp. 539-542, March 2009.

7. A. A. Fock and P. M. Hart, "New method for measuring X_d and X_q based on the P-Q diagram of the lossy salient-pole machine", *IEE Proceedings B: Electric Power Applications*, Vol. 131, Issue 6, pp. 259 – 262, November 1984.